 CMES, vol.4, no.5, pp.571-585, 2003

Application of Meshless Local Petrov-Galerkin (MLPG) to Problems with Singularities, and Material Discontinuities, in 3-D Elasticity

Q. Li[1], S. Shen[1], Z. D. Han[1], and S. N. Atluri[1]

Abstract: In this paper, a truly meshless method, the Meshless Local Petrov-Galerkin (MLPG) Method, is developed for three-dimensional elasto-statics. The two simplest members of MLPG family of methods, the MLPG type 5 and MLPG type 2, are combined, in order to reduce the computational requirements and to obtain high efficiency. The MLPG5 method is applied at the nodes inside the 3-D domain, so that any domain integration is eliminated altogether, if no body forces are involved. The MLPG 2 method is applied at the nodes that are on the boundaries, and on the interfaces of material discontinuities, so that the boundary conditions, and material discontinuities, are satisfied without any further tedious integration. Two classical three-dimensional elasto-statics problems, viz., the Boussinesq problem, and the Eshelby's inclusion problem, are analyzed with the current method. The MLPG results agree excellently with the analytical solutions, and demonstrate their superiority over the results obtained from the traditional displacement-finite-element method. The MLPG method is straightforward, easy to implement, efficient, and accurate; therefore it holds a great promise to replace the finite element method in three-dimensional analysis in the near future.

keyword: meshless method, Meshless Local Petrov-Galerkin (MLPG) methods, local symmetric weak form, Moving Least Squares (MLS) interpolation

1 Introduction

Meshless methods have received a lot of attention in the past decade, due to their potential in eliminating the costly effort of mesh generation. A variety of meshless methods has been proposed; for example, the diffuse element method by Nayroles, Touzot, and Villon (1992); element free Galerkin method by Belytschko, Lu, and Gu (1994); reproducing kernel particle method by Liu, Chen, Uras, and Chang (1996); partition of unity finite element method by Babuska and Melenk (1997); HP cloud method by Duarte and Oden (1996). However, most of the methods require the use of background cells for the integration of weak form. Therefore, these methods are not truly mesh free.

It is also noteworthy that meshless methods have found very limited application to three-dimensional analysis, which is a routine application for the finite element method. The major reason lies in the complicated nature of the meshless interpolation, which makes the 3D application numerically demanding. Berry and Saigal (1999) applied the element free Galerkin method to three-dimensional elasto-static problems. However, both domain integration and boundary integration were involved in their formulation, which required a lot of computing power, and thus, they limited their application to simple examples. Also, as mentioned before, background cells were inevitably involved in the integration of the weak form.

On the other hand, the Meshless Local Petrov-Galerkin (MLPG) approach is a truly meshless method, which requires no elements or "background cells" in either interpolation or integration [Atluri and Zhu (1998)]. In the MLPG method, the integrations of the weak form are performed over local sub-domains that overlap with each other. The trial functions and the test functions are chosen from totally different functional spaces. Furthermore, the physical size of the test domain and trial domain are not necessary to be the same, which makes the MLPG method a very flexible method. By selecting different trial functions and test functions, the MLPG method could be classified into six different types, which are labeled as MLPG1, MLPG2, MLPG3, MLPG4, MLPG5, and MLPG6 [Atluri and Shen (2002 a, b)]. The MLPG methods have found a wide range of appli-

[1] Center for Aerospace Education & Research
University of California, Irvine
5251 California Ave., Suite 140
Irvine, CA 92612, USA

cation in elasto-statics [Atluri and Zhu (2000)], elasto-dynamics [Batra and Ching (2002)], fluid mechanics [Lin and Atluri (2001)], convection-diffusion problem [Lin and Atluri (2000)], thermoelasticity [Sladek, Sladek and Atluri 2001], beam problems [Raju and Phillips (2003)], plate problems [Gu and Liu (2001), Long and Atluri (2002), Qian, Batra and Chen (2003)], fracture mechanics [Kim and Atluri (2000), Ching and Batra (2001)], and strain gradient theory [Tang, Shen and Atluri (2003)].

Among the six MLPG methods, the MLPG 5 (wherein the local, nodal-based test function, over a local sub-domain centered at a node, is the Heaviside step function) eliminates the necessity of domain integration, and shows high robustness and accuracy in two dimension analysis [Atluri and Shen (2002 a, b)]. By applying the MLPG 5 to 3-D elasticity, we obtain in this paper, a straightforward and efficient program that holds great promise to replace the finite element method for three-dimensional solid mechanics.

In order to further increase the efficiency, the MLPG 2 (wherein the local, nodal-based test function, over a local sub-domain centered at a node, is the Dirac's delta function) is used in the treatment of boundary-conditions, and of material discontinuities. Therefore, numerical integrations are no longer involved in the enforcement of boundary conditions, of conditions of material discontinuity. By combining the MLPG 2 and MLPG 5 methods, the boundary conditions are easily enforced, and any material discontinuity can be accurately simulated.

2 The MLPG 5 Formulation for Three-Dimensional Elasticity

The equations of equilibrium in a volume Ω bounded by surface Γ, are given by

$$\sigma_{ij,j} + b_i = 0 \qquad \text{in} \quad \Omega \tag{1}$$

where σ_{ij} is the stress tensor and b_i are the body forces. On the boundary Γ, it is also assumed that:

$$u_i = \overline{u}_i \qquad \text{on} \quad \Gamma_u \tag{2}$$

$$\sigma_{ij} n_j = \overline{t}_i \qquad \text{on} \quad \Gamma_t \tag{3}$$

where $\overline{u}_i$ are the prescribed displacements, $\overline{t}_i$ are the prescribed surface tractions, n_j is the outward normal of the global boundary, Γ_u is the global boundary with prescribed displacements and Γ_t is the global boundary with prescribed surface tractions.

Instead of writing the global weak form for the above equilibrium equations, the MLPG methods construct the weak-form over local sub-domains such as Ω_s, which is a small region taken for each node inside the global domain (Figure1.a). The local sub-domains overlap each other, and cover the whole global domain Ω (Figure1.b). The local sub-domains could be of any geometric shape and size; however, in the current paper, the local sub-domains are taken to be of spherical shape, for numerical simplicity. The local weak form of the equilibrium equations over the sub-domain around node I is listed in equation (4):

$$\int_{\Omega_s^I} (\sigma_{ij,j} + b_i) v_i d\Omega_s - \alpha \int_{\Gamma_{su}^I} (u_i - \overline{u}_i) v_i d\Gamma = 0 \tag{4}$$

where v_i is the test function. The penalty parameter α is introduced in order to satisfy the geometric boundary condition. Using $\sigma_{ij,j} v_i = (\sigma_{ij} v_i)_{,j} - \sigma_{ij} v_{i,j}$ and the divergence theorem, we have

$$\int_{\partial\Omega_s^I} \sigma_{ij} n_j v_i d\Gamma - \int_{\Omega_s^I} (\sigma_{ij} v_{i,j} - b_i v_i)\, d\Omega - \alpha \int_{\Gamma_{su}^I} (u_i - \overline{u}_i) v_i d\Gamma = 0 \tag{5}$$

where $\partial\Omega_s^I$ is the boundary of the local sub-domain, which consists of three parts, $\partial\Omega_s^I = L_s^I \cup \Gamma_{st}^I \cup \Gamma_{su}^I$. L_s^I is the local boundary that is totally inside global domain, Γ_{st}^I is the part of local boundary that coincides with the global traction boundary, i.e., $\Gamma_{st}^I = \partial\Omega_s^I \cap \Gamma_t$, and Γ_{su}^I is part of local boundary that coincides with the global geometric boundary, i.e., $\Gamma_{su}^I = \partial\Omega_s^I \cap \Gamma_u$. Writing equation (5) in terms of L_s^I, Γ_{st}^I, and Γ_{su}^I and applying the natural boundary condition $t_i = \sigma_{ij} n_j = \overline{t}_i$.

$$\int_{L_s^I} t_i v_i d\Gamma + \int_{\Gamma_{su}^I} t_i v_i d\Gamma + \int_{\Gamma_{st}^I} \overline{t}_j v_i d\Gamma - \int_{\Omega_s^I} (\sigma_{ij} v_{i,j} - b_i v_i)\, d\Omega - \alpha \int_{\Gamma_{su}^I} (u_i - \overline{u}_i) v_i d\Gamma = 0 \tag{6}$$

Rearranging the terms, we obtain the *local symmetric*

weak form (LSWF) in linear elasticity:

$$\int_{\Omega_s^I} \sigma_{ij} v_{i,j} d\Omega - \int_{L_s^I} t_i v_i d\Gamma - \int_{\Gamma_{su}^I} t_i v_i d\Gamma + \alpha \int_{\Gamma_{su}^I} u_i v_i d\Gamma = \int_{\Gamma_{st}^I} \bar{t}_j v_i d\Gamma + \alpha \int_{\Gamma_{su}^I} \bar{u}_i v_i d\Gamma + \int_{\Omega_s^I} b_i v_i d\Omega \tag{7}$$

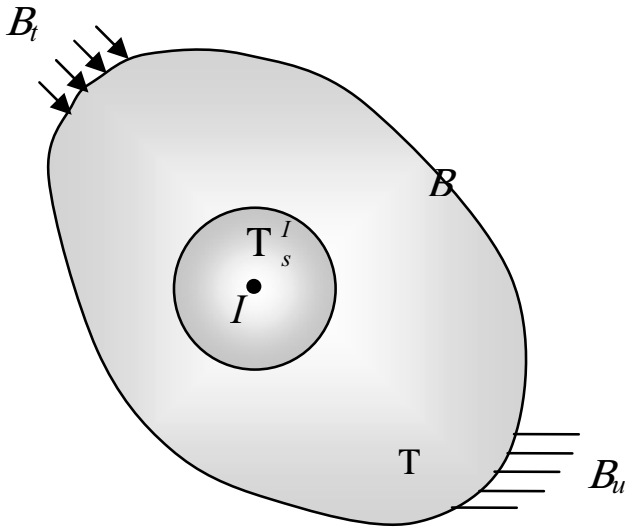

Figure 1a : Definition of the Local Sub-domain

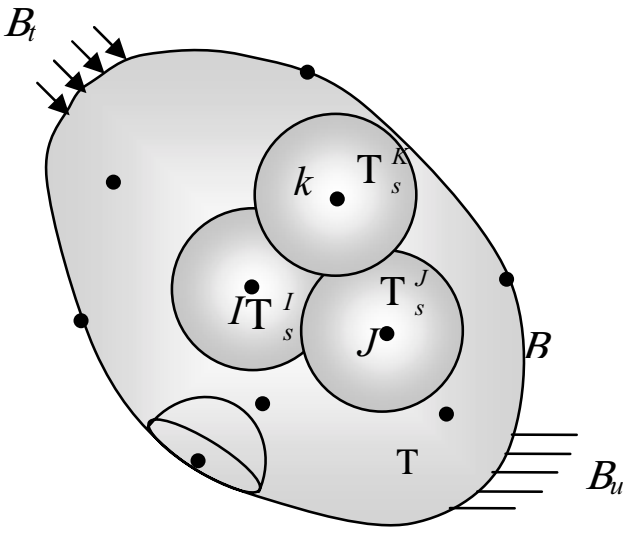

Figure 1b : Overlapping Local Sub-domain Covering the Global Domain

If a Heaviside step function is chosen as the test function in each sub-domain, a method which is recognized as MLPG 5 method in Atluri and Shen (2002 a, b) results, and the above LSWF is simplified as:

$$-\int_{L_s^I} t_i d\Gamma - \int_{\Gamma_{su}^I} t_i d\Gamma + \alpha \int_{\Gamma_{su}^I} u_i d\Gamma = \int_{\Gamma_{st}^I} \bar{t}_j d\Gamma + \alpha \int_{\Gamma_{st}^I} \bar{u}_i d\Gamma + \int_{\Omega_s^I} b_i d\Omega \tag{8}$$

$$v(x) = \begin{cases} 1 \text{ at } x \in \Omega_S \\ 0 \text{ at } x \notin \Omega_S \end{cases} \tag{9}$$

It is seen that in equation (8), there is no domain integration involved in the left hand side, which leads to the stiffness matrix, after discretization. If the assumption of zero body force is made, then domain integration is totally eliminated.

3 The Physical Interpretation of MLPG 5 method for 3-D Solid Mechanics

Suppose we consider a sub-domain Ω_s^I, centered at node I; and further suppose that Ω_s^I is entirely within the domain of the solid Ω. Thus, in this case $\partial\Omega_s^I \equiv L_s^I$.

Hence, equation (8) reduces to

$$\int_{\partial\Omega_s^I} t_i d\Gamma + \int_{\Omega_s^I} b_i d\Omega = 0 \tag{10}$$

which is immediately recognized as nothing more than the overall equilibrium of the sub-domain Ω_s^I. Furthermore, we consider the displacement continuity, and traction reciprocity between the domains Ω_s^I and $\Omega - \Omega_s^I$, respectively, as:

$$u_i^+|_{\text{at the boundary of } \Omega_s^I} \equiv u_i^-|_{\text{at the internal boundary of } \Omega - \Omega_s^I \text{ which interfaces with } \Omega_s^I} \tag{11a}$$

and

$$t_i^+|_{\text{at the boundary of } \Omega_s^I} \equiv t_i^-|_{\text{at the internal boundary of } \Omega - \Omega_s^I \text{ which interfaces with } \Omega_s^I} \tag{11b}$$

For the moment, we assume that the material properties are continuous between Ω_s^I and $\Omega - \Omega_s^I$. Thus, if a moving least square approximation discussed in next section

is assumed such that it is at least of C^1 continuity, then it is easily seen that equations (11a) and (11b) are identically satisfied by the trial functions.

Thus, the MLPG5 method [Atluri and Shen (2002 a, b)] can simply be interpreted as nothing more than enforcing the overall momentum balance laws of mechanics, over each sub-domain Ω_s^I; as well as enforcing the displacement continuity and traction reciprocity conditions between Ω_s^I and $\Omega - \Omega_s^I$ identically. This interpretation clearly enables one to develop the MLPG method very easily for nonlinear solid mechanics, in solving large displacement gradients, large rotations, large strains and material inelastic behavior including plasticity, viscoplasticity, and creep.

4 Three Dimensional Moving Least Square (MLS) Approximation

As mentioned above, in the MLPG method, the test and trial function are not necessarily from the same spaces. For internal nodes, the Heaviside step function, over each local sub-domain, is chosen to be the test function. The trial function, on the other hand, is chosen to be the moving least square (MLS) interpolation over a number of nodes within the domain of influence. While the local sub-domain is defined as the support of the test function on which the integration is carried out, the domain of influence is defined as a region where the weight function of the node inside of it doesn't not vanish in the local sub-domain of the current node. In other words, the domain of influence contains all the nodes that have non-zero coupling with the current nodal values in the stiffness matrix (Figure 2).

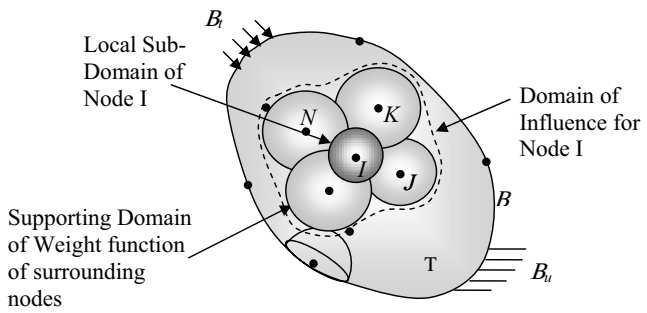

Figure 2 : MLPG Trial and Test Domain

In figure 2, the sphere surrounding node I represents the local sub-domain where the integration is carried out. The spheres surrounding node J, K, L, M... represent the supporting domain of weight functions of nodes, whose weight functions do not vanish in the local sub-domain. The volume surrounded by dashed curve represents the domain of influence of node I. In general, the size of the domain of influence has to be large enough in order to ensure continuity.

The MLS method is generally considered to be one of the useful interpolation schemes that approximate random data with reasonable accuracy. The characteristic of MLS has been widely discussed in literatures [Atluri, Kim, and Cho (1999), Breikopf, Rassineux, Touzot and Villon (2000), Jin, Li and Aluru (2001)]. The three dimensional MLS follows the same methodology as in two dimension formulations, while the interpolation basis has been extended into three dimensional spaces.

The MLS approximation of u for any point $\mathbf{x} \in \Omega_s^I$, is defined by

$$u^h = \mathbf{p}^{\mathbf{T}}(\mathbf{x})\mathbf{a}(\mathbf{x}) \quad \mathbf{x} \in \Omega_s^I \tag{12}$$

where $\mathbf{p}^{\mathbf{T}}(\mathbf{x}) = [p_1(\mathbf{x}), p_2(\mathbf{x}), ..., p_m(\mathbf{x})]$ is a complete monomial basis of order m. In three dimension problem the linear basis is defined as

$$\mathbf{p}^{\mathbf{T}}(\mathbf{x}) = [1, x, y, z] \tag{13}$$

the quadratic basis is defined as

$$\mathbf{p}^{\mathbf{T}}(\mathbf{x}) = \left[1, x, y, z, x^2, y^2, z^2, xy, yz, zx\right] \tag{14}$$

a(x) is a coefficient vector which is defined by minimizing a weighted discrete L_2-norm

$$\begin{aligned} J(\mathbf{a}(\mathbf{x})) &= \sum_{I=1}^{N} w_I(\mathbf{x}) \left[\mathbf{p}(\mathbf{x_I})\mathbf{a}(\mathbf{x}) - \hat{u}^I\right]^2 \\ &= [\mathbf{P}\cdot\mathbf{a}(\mathbf{x}) - \hat{\mathbf{u}}]^T \cdot \mathbf{W}(\mathbf{x}) \cdot [\mathbf{P}\cdot\mathbf{a}(\mathbf{x}) - \hat{\mathbf{u}}] \end{aligned} \tag{15}$$

where $\mathbf{x}_I$ is the position of the Ithnode whose weight function w_I does not vanish at $\mathbf{x}$.

$$\mathbf{P} = \begin{bmatrix} \mathbf{p}^{\mathbf{T}}(\mathbf{x}_1) \\ \mathbf{p}^{\mathbf{T}}(\mathbf{x}_2) \\ \cdots \\ \mathbf{p}^{\mathbf{T}}(\mathbf{x}_N) \end{bmatrix}_{N\times m},$$

$$\mathbf{W} = \begin{bmatrix} w_1(\mathbf{x}) & \cdots & 0 \\ \vdots & \ddots & \vdots \\ 0 & \cdots & w_N(\mathbf{x}) \end{bmatrix}_{N\times N},$$

$$\hat{\mathbf{u}} = \left[\hat{u}^1, \hat{u}^2, \cdots, \hat{u}^N\right]_{1\times N}$$

where $\hat{u}^I$, $I = 1, 2, \ldots, N$ are the fictitious nodal value. It needs to be mentioned that in MLS interpolation, the fictitious nodal value $\hat{u}^I$ does not equal to the approximated value u^h. The stationary condition of $J(\mathbf{x})$ with respect to the coefficients **a(x)** leads to the following linear relation

$$\mathbf{A}(\mathbf{x})_{m\times m}\mathbf{a}(\mathbf{x})_{m\times 1} = \mathbf{B}(\mathbf{x})_{m\times N}\hat{\mathbf{u}}_{N\times 1} \tag{16}$$

where

$$\mathbf{A}(\mathbf{x}) = \mathbf{P^T W P} = \sum_{\mathbf{I=1}}^{\mathbf{N}} w_I \mathbf{p}(\mathbf{x_I})\mathbf{p^T}(\mathbf{x_I}) \tag{17}$$

$$\begin{aligned}\mathbf{B}(\mathbf{x}) &= \mathbf{P^T W}\\ &= [w_1(\mathbf{x})\mathbf{p}(\mathbf{x}_1), w_2(\mathbf{x})\mathbf{p}(\mathbf{x}_2), \ldots, w_N(\mathbf{x})\mathbf{p}(\mathbf{x}_N)]\end{aligned}$$

By substituting **a(x)** into equation (12), the interpolation function $u^h(\hat{u}^I)$ is obtained

$$u^h = \sum_{I=1}^{N} \phi^I(\mathbf{x})\hat{u}^I \tag{18}$$

where $\phi^I(\mathbf{x}) = \sum_{j=1}^{m} p_j(\mathbf{x})\left[\mathbf{A}^{-1}(\mathbf{x})\mathbf{B}(\mathbf{x})\right]_{jI}$

In the current paper, a 4^{th} order spline type weight function is used

$$w_I(\mathbf{x}) = \begin{cases} 1-6\left(\frac{d_I}{r_I}\right)^2 + 8\left(\frac{d_I}{r_I}\right)^3 - 3\left(\frac{d_I}{r_I}\right)^4 & 0 \le d_I \le r_I \\ 0 & d_I \ge r_I \end{cases} \tag{19}$$

It is seen that C^1 continuity is ensured over the entire domain, therefore the traction reciprocity $t^- + t^+ = 0$ is automatically strongly satisfied in the present method.

5 Numerical Discretization

By substituting the MLS interpolation function (18) into the MLPG 5 formulation (8), the following discretized system of linear equations is obtained:

$$\begin{aligned}&-\sum_{J=1}^{N}\int_{L_s^I}\mathbf{NDB^J}\hat{\mathbf{u}}^{\mathbf{J}}d\Gamma - \sum_{J=1}^{N}\int_{\Gamma_{su}^I}\mathbf{SNDB^J}\hat{\mathbf{u}}^{\mathbf{J}}d\Gamma\\ &+\alpha\sum_{J=1}^{N}\int_{\Gamma_{su}^I}\mathbf{S}\boldsymbol{\Phi}^{\mathbf{J}}\hat{\mathbf{u}}^{\mathbf{J}}d\Gamma\\ &=\int_{\Gamma_{st}^I}\bar{\mathbf{t}}d\Gamma+\alpha\int_{\Gamma_{su}^I}\bar{\mathbf{u}}d\Gamma+\int_{\Omega_s^I}\mathbf{b}d\Omega\end{aligned} \tag{20}$$

where, in three-dimensional space,

$$\mathbf{N} = \begin{bmatrix} n_1 & 0 & 0 & n_2 & 0 & n_3 \\ 0 & n_2 & 0 & n_1 & n_3 & 0 \\ 0 & 0 & n_3 & 0 & n_2 & n_1 \end{bmatrix},$$

$$\mathbf{B^J} = \begin{bmatrix} \phi^J_{,1} & 0 & 0 \\ 0 & \phi^J_{,2} & 0 \\ 0 & 0 & \phi^J_{,3} \\ \phi^J_{,2} & \phi^J_{,1} & 0 \\ 0 & \phi^J_{,3} & \phi^J_{,2} \\ \phi^J_{,3} & 0 & \phi^J_{,1} \end{bmatrix}, \quad \boldsymbol{\Phi}^{\mathbf{J}} = \begin{bmatrix} \phi^J & 0 & 0 \\ 0 & \phi^J & 0 \\ 0 & 0 & \phi^J \end{bmatrix}$$

$$\hat{\mathbf{u}}^{\mathbf{J}} = \begin{Bmatrix} \hat{u}_1^J \\ \hat{u}_2^J \\ \hat{u}_3^J \end{Bmatrix}, \quad \mathbf{S} = \begin{bmatrix} S_1 & 0 & 0 \\ 0 & S_2 & 0 \\ 0 & 0 & S_3 \end{bmatrix}$$

with $S_i = \begin{cases} 1 & \text{if } u_i \text{ is prescribed on } \Gamma_u \\ 0 & \text{if } u_i \text{ is not prescribed on } \Gamma_u \end{cases}$, $i = 1,3$

$$\mathbf{D} = D_0\begin{bmatrix} 1 & \frac{\nu}{1-\nu} & \frac{\nu}{1-\nu} & 0 & 0 & 0 \\ \frac{\nu}{1-\nu} & 1 & \frac{\nu}{1-\nu} & 0 & 0 & 0 \\ \frac{\nu}{1-\nu} & \frac{\nu}{1-\nu} & 1 & 0 & 0 & 0 \\ 0 & 0 & 0 & \frac{1-2\nu}{2(1-\nu)} & 0 & 0 \\ 0 & 0 & 0 & 0 & \frac{1-2\nu}{2(1-\nu)} & 0 \\ 0 & 0 & 0 & 0 & 0 & \frac{1-2\nu}{2(1-\nu)} \end{bmatrix}$$

with $D_0 = \dfrac{E(1-\nu)}{(1+\nu)(1-2\nu)}$

(n_1, n_2, n_3) is the outward normal on the boundary of local sub-domain, E and ν are the Young's modulus and Poisson's ratio, respectively. If MLPG 5 is applied to internal nodes, whose sub-domains do not intersect with the global boundary, then the governing equation is simplified to

$$-\sum_{J=1}^{N}\int_{L_s^I}\mathbf{NDB^J}\hat{\mathbf{u}}^{\mathbf{J}}d\Gamma = \int_{\Omega_s^I}\mathbf{b}d\Omega \tag{21}$$

in a short form

$$\sum_{J=1}^{N}\mathbf{K_{IJ}}\hat{\mathbf{u}}^{\mathbf{J}} = \mathbf{f_I} \tag{22}$$

where

$$\mathbf{K_{IJ}} = -\int_{L_s^I}\mathbf{NDB^J}d\Gamma, \quad \mathbf{f_I} = \int_{\Omega_s^I}\mathbf{b}d\Omega$$

6 Treatment of Boundary Conditions and Material Discontinuities

In order to make the three-dimensional MLPG to be an efficient and accurate method, it is crucial to simplify the calculations, while maintaining a high accuracy. Although domain integration is no longer involved in calculating the stiffness matrix in equation (20), the three-dimensional boundary integration is still numerically demanding for boundary nodes. The geometric shapes of L_s^I, Γ_{st}^I, and Γ_{su}^I need to be calculated and then integrated upon. For three-dimensional continuous media with arbitrary geometric configurations, the above geometric calculations are usually tedious, and to integrate over them requires even larger amount of computing effort. Hence, a different treatment is necessary for the nodes on the boundary, as compared with the nodes located inside the domain.

Material discontinuities, on the other hand, are a well-known drawback of the meshless method, with an inherently higher-order-continuous displacement field. Because of the highly continuous trial function which is at least C^1, it is difficult to simulate "jumps" in the strain field. Therefore, a special treatment is also applied at the location of material discontinuities.

6.1 The Treatment of Boundary Nodes

Before we move on to the topic of the treatment of boundary nodes, first we need to clarify the definition of boundary nodes in the current method. The "boundary nodes" are defined as the nodes that are located exactly on the global boundary Γ (Figure 3.a). For the nodes that are located close to the global boundary but not exactly on the boundary, the radius of local sub-domain is adjusted so that the sub-domains for such nodes would not cross over the global boundary (Figure 3.b). These nodes form a "boundary layer" that is lining the surface of the global boundary. As a result, there are only two types of nodes in the current method. The first type are the internal nodes whose local sub-domains have no intersection with the global boundary. The governing equations of these internal nodes are defined by equation (22). For internal nodes, boundary integrations are easily carried out because the local sub-domains are pure spheres. The second type are the boundary nodes, which are located exactly on the global boundary Γ. The local sub-domains of these nodes thus intersect with the global boundary Γ. In order to avoid integrations over these intersections, a special treatment of the boundary nodes is introduced as follows:

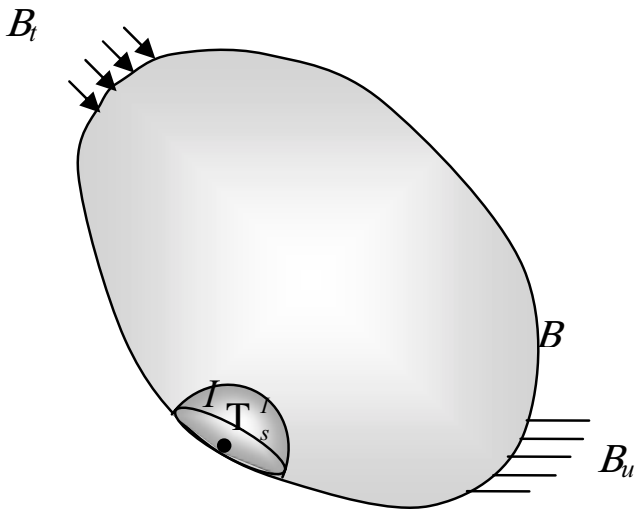

Figure 3a : Definitions of Boundary Nodes

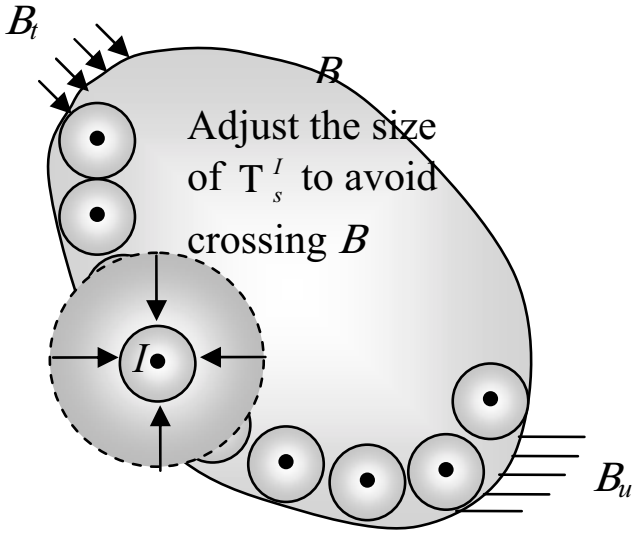

Figure 3b : Adjustment of Internal Nodes to Form a "Boundary Layer"

There has been a lot of work in the meshless method, on the topic of boundary conditions, especially the enforcement of essential boundary condition [Mukherjee and Mukherjee (1997)]. Zhu and Atluri (1998) proposed a modified collocation method that enforced the essential boundary condition directly at the collocation points.

Following this, we choose a Dirac's Delta function as the test function (MLPG 2) for boundary nodes, instead of the Heaviside step function, as in MLPG 5.

$$v_i = \delta(x - x_i) \tag{23}$$

The boundary conditions simply become

$$(u_i - \overline{u}_i) = 0 \qquad \text{for nodes located on } \Gamma_{su}^I \tag{24}$$

$$(t_i - \overline{t}_i) = 0 \qquad \text{for nodes located on } \Gamma_{st}^I \tag{25}$$

After substituting equation (18) into (24) and (25), we obtain a discretized system of linear equation for the boundary nodes

$$\sum_{J=1}^{N} \phi^J \hat{\mathbf{u}}^J = \overline{\mathbf{u}} \qquad \text{for nodes located on } \Gamma_{su}^I \tag{26}$$

$$\sum_{J=1}^{N} \mathbf{NDB}^J \hat{\mathbf{u}}^J = \overline{\mathbf{t}} \qquad \text{for nodes located on } \Gamma_{st}^I \tag{27}$$

Or, in a short form, the nodal equations become

$$\sum_{J=1}^{N} \mathbf{K}_{IJ} \hat{\mathbf{u}}^J = \mathbf{f}_I \tag{28}$$

where

$$\mathbf{K}_{IJ} = \phi^J \delta_{IJ}, \quad \mathbf{f}_I = \overline{\mathbf{u}} \qquad \text{for nodes on } \Gamma_{su}^I \tag{29}$$

$$\mathbf{K}_{IJ} = \mathbf{NDB}^J, \quad \mathbf{f}_I = \overline{\mathbf{t}} \qquad \text{for nodes on } \Gamma_{st}^I \tag{30}$$

Equations (28) $\sim$ (30) are the governing equations for the boundary nodes. Both the essential and natural boundary conditions are satisfied in the weak form on the collocation nodes. It is clear that there is no numerical integration necessary for the boundary nodes at all. Although a different type of test functions are adopted for the nodes at the boundary, and the internal nodes, respectively, there is no problem for the two types of nodes to present in the same domain of influence and interpolated upon. By combining the methods of MLPG 5 and MLPG 2 together, the implementation is simplified and the calculation is accelerated significantly.

6.2 Treatment of Material Discontinuities

Like most of the other meshless approximations, the MLPG method naturally leads to continuously differentiable approximations, often of the C^1 type, so that the partial derivatives of the approximation, i.e. strains and stresses in elastic problem, are smooth and require no post-processing. However, this highly continuous nature also leads to difficulty when there is an imposed discontinuity in the derivatives, such as the natural discontinuity in strains when material discontinuities are present. There has been a lot of effort devoted to solving this problem. Krongauz and Belytschko (1998) introduced a "jump shape function", a trial function with a pre-imposed discontinuity in the gradient of the function, at the location of the material discontinuity, in addition to the MLS approximation, in order to simulate the discontinuity in strain field for 2-D elastic problem. However, this method requires interpolation in the curvelinear coordinates, which becomes very tedious in three dimensional applications. Cordes and Moran (1996) also solved the problem in 2-D elasticity by using Lagrange multiplier; however, their method required both domain integrations and boundary integrations on the surface of discontinuity, which requires a lot of computational effort when the discontinuity is of an arbitrary geometrical shape.

A much more straightforward method is developed here in order to solve the three dimensional problem with material discontinuity, i.e., a problem with a strain discontinuity across an arbitrary curved surface in three-dimensional space. The inhomogeneous medium is considered separately as several homogeneous bodies. Two sets of collocation nodes are assigned on both the + side and the – side of material interface at the same location, but with different material properties. The MLS interpolation is carried out separately within each of the homogeneous domains, so that the domain of influence is truncated at the interface of the two media. Therefore, the high order continuity is kept within each of the same homogeneous media, but not across the interface between the two different media.

For the nodes that are close to but not exactly on the material interface, their local sub-domains are adjusted so as not to cross over the interface boundary. The MLPG 5 is applied to the nodes that are not the on the material interface, the boundary integration is of simple form because the spherical shape of local sub-domain is guar-

anteed (Figure 4).

Because there are only collocation nodes on the material interface, combining the separate homogeneous media in the weak form, becomes as simple as:

$$\begin{cases} \mathbf{u}^+ = \mathbf{u}^- & \text{displacement continuity at the interface} \\ \mathbf{t}^+ + \mathbf{t}^- = 0 & \text{traction reciprocity at the interface} \end{cases} \tag{31}$$

In matrix form

$$\sum_{J=1}^{N^+} \phi^J \hat{\mathbf{u}}^J - \sum_{I=1}^{N^-} \phi^I \hat{\mathbf{u}}^I = 0 \qquad \text{on} \quad \Gamma_i^K \tag{32}$$

$$\sum_{J=1}^{N^+} \mathbf{NDB}^J \hat{\mathbf{u}}^J + \sum_{I=1}^{N^-} \mathbf{NDB}^I \hat{\mathbf{u}}^I = 0 \qquad \text{on} \quad \Gamma_i^K \tag{33}$$

where N^+ is the number of nodes in the medium +, whose domains of influence do not vanish at the location of interface node K. N^- is the number of nodes in the medium –, whose domains of influence do not vanish at the location of interface node K.

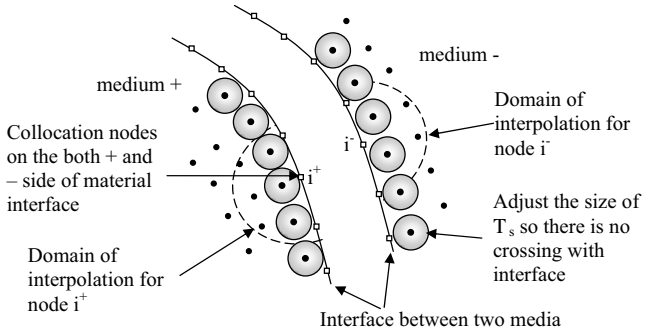

Figure 4 : The Treatment of Material Discontinuity

7 Numerical Experiments

Numerical experiments have been performed in order to illustrate the effectiveness of the current method. The three-dimensional Boussinesq problem is solved first, in order to evaluate the performance of the current method in problems with singular displacements as well as singular stress fields. The Eshelby's inclusion problem is also solved, to evaluate the performance of current method, when there is a material discontinuity. In all the examples, the body force is set to be zero. The convergence rate of the method is also studied. In the calculation of relative error, the displacement L_2-norm, Von Mises stress L_2-norm, and energy L_2-norm are defined as follows:

$$\|\mathbf{u}\| = \left(\int_\Omega \mathbf{u}^\mathbf{T} \cdot \mathbf{u} d\Omega \right)^{\frac{1}{2}} \tag{34}$$

$$\|\sigma_e\| = \left(\int_\Omega \sigma_e^2 d\Omega \right)^{\frac{1}{2}} \tag{35}$$

$$\|\varepsilon\| = \left(\frac{1}{2} \int_\Omega \varepsilon^\mathbf{T} \cdot \mathbf{D} \cdot \varepsilon d\Omega \right)^{\frac{1}{2}} \tag{36}$$

The relative errors in displacement, Von Mises stress, and energy are defined as

$$r_u = \frac{\|\mathbf{u}^{num} - \mathbf{u}^{exact}\|}{\|\mathbf{u}^{exact}\|} \tag{37}$$

$$r_s = \frac{\|\sigma_e^{num} - \sigma_e^{exact}\|}{\|\sigma_e^{exact}\|} \tag{38}$$

$$r_e = \frac{\|\varepsilon^{num} - \varepsilon^{exact}\|}{\|\varepsilon^{exact}\|} \tag{39}$$

7.1 Three Dimensional Boussinesq Problem

The Boussinesq problem is a classical problem for the study of contact, penetration, and impact problems. The problem can simply be described as a concentrated load acting on a semi-infinite elastic medium with no body force (Figure 5). Because of the strong singularity in the Boussinesq problem, it is very difficult to get an accurate result using domain discretization methodology such as the finite element method.

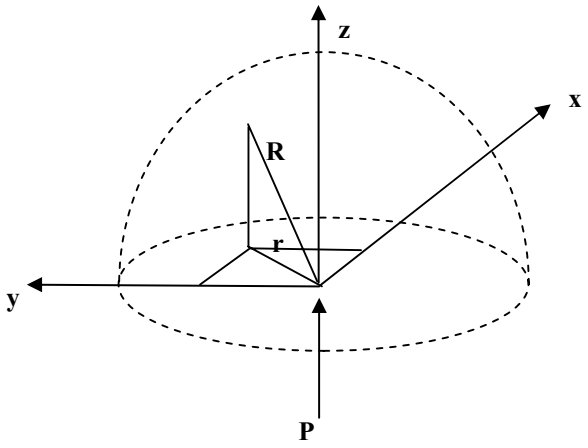

Figure 5 : Bossinesq Problem

The exact displacement field within the semi-infinite medium is given by [Timoshenko & Goodier (1951)]

$$\begin{cases} u_r = \frac{(1+\nu)P}{2E\pi R}\left[\frac{zr}{R^2} - \frac{(1-2\nu)r}{R+z}\right] \\ w = \frac{(1+\nu)P}{2E\pi R}\left[\frac{z^2}{R^2} + 2(1-\nu)\right] \end{cases} \tag{40}$$

where u_r is the radial displacement, w is the vertical displacement, R is the distance to the loading point, r is the projection of R on the loading surface.

The theoretical stresses field is in

$$\begin{cases} \sigma_r = \frac{P}{2\pi R^2}\left[-\frac{3r^2 z}{R^3} + \frac{(1-2\nu)R}{R+z}\right] \\ \sigma_\theta = \frac{(1-2\nu)P}{2\pi R^2}\left[\frac{z}{R} - \frac{R}{R+z}\right] \\ \sigma_z = -\frac{3Pz^3}{2\pi R^5} \\ \tau_{zr} = \tau_{rz} = -\frac{3Prz^2}{2\pi R^5} \end{cases} \tag{41}$$

It is clear that the displacements and stresses are strongly singular and approach to infinity; with the displacement being $O(\frac{1}{R})$ and the stresses being $O(\frac{1}{R^2})$.

A one-eighth of a sphere is used to simulate the semi-infinite medium. In order to avoid direct encounter with the singular loading point, the theoretical displacement is applied on a small spherical surface with a radius as low as 2.5% of the total radius of the sphere. Symmetric boundary conditions are applied on the surfaces of the one-eighth sphere (Figure 6).

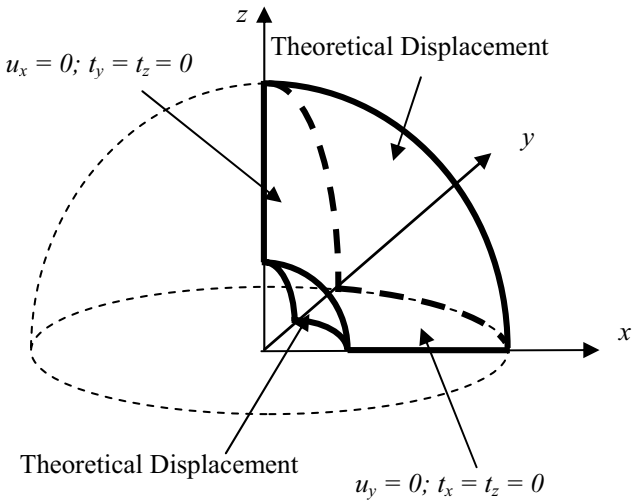

Figure 6 : Simulation Model for the Boussinesq Problem

An isotropic material of E = 1000 and ν = 0.25 is used in the simulation. Three models with node numbers of 1177, 2641, and 3939 are simulated. Three finite element models with 1159 nodes, 3683 nodes and 11112 nodes are also developed for comparison purpose. The 1177 node MLPG model and 1159 node FEM model are shown in figure 7.a and 7.b. Both the node numbering and the nodal distances are similar for the two models.

The 3939 node MLPG model, and the 11112 node FEM model are shown in Figure 7.c and 7.d. The two models have similar nodal distances at the stress-concentrated area; however, it can be seen that a lot more nodes need to be added in FEM model in order to prevent element distortion and to maintain a reasonable element aspect ratio. With 3939 nodes, the MLPG method can achieve a minimum nodal distance of 0.015, while the finite element method requires more than ten thousand nodes to obtain the similar nodal distance.

The radial displacement u_r and vertical displacement w on the z = 0 surface of the 3939 node MLPG model are shown in figure 8.a. The Von Mises stress on the z = 0 surface of the 3939 node MLPG model is shown in figure 8.b. The analytical solution for the displacement and stress are plotted on the same figures for comparison purpose. It can be seen that both the MLPG displacement and stress results match the analytical solution accurately.

Because *the displacement is prescribed on the boundary*, both MLPG and FEM give a low displacement error of 1% to 2% percent. However, the relative errors of Von Mises stress in the MLPG analysis range from 1.17% to 2.63%, which are about two to three times lower compared to the FEM result of similar minimum nodal distance (Figure 9.a). The strain energy relative errors of MLPG range from 2.32% to 4.86%, which are about three to four times lower then the FEM result (Figure 9.b).

On figure 9.c, the relative errors of Von Mises stress and strain energy for both MLPG and FEM method are plotted on the same figure. It can be seen that even with a node number as high as 11112, the accuracy of the finite element method is still far less then the MLPG method.

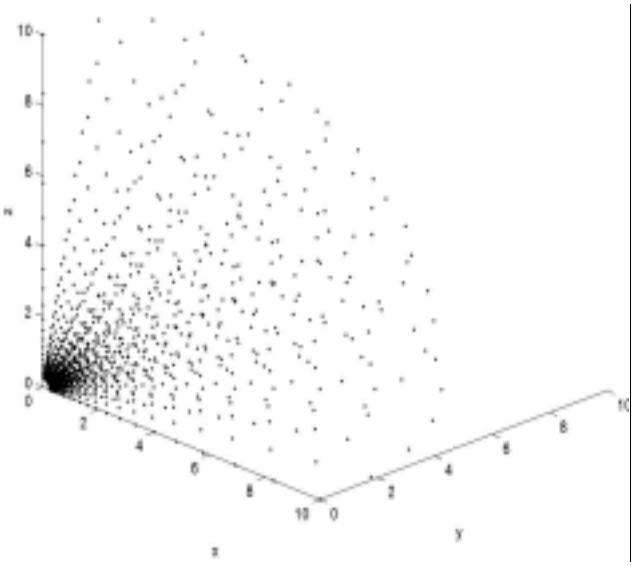

Figure 7a : MLPG Model with 1177 Nodes for Boussinesq Problem

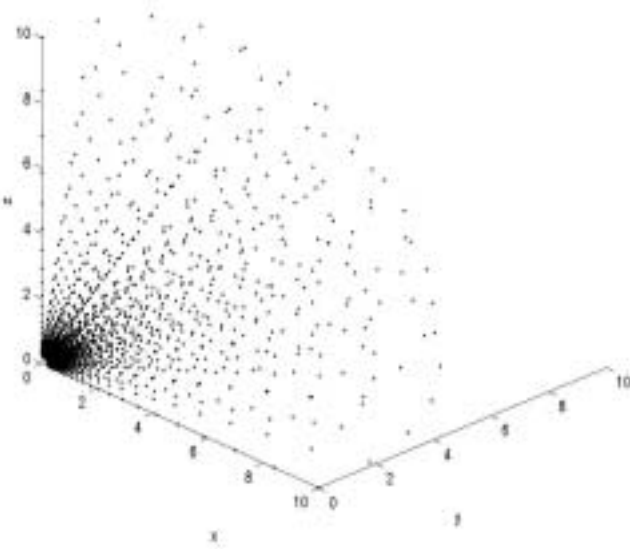

Figure 7c : MLPG Model with 3939 Nodes for Boussinesq Problem

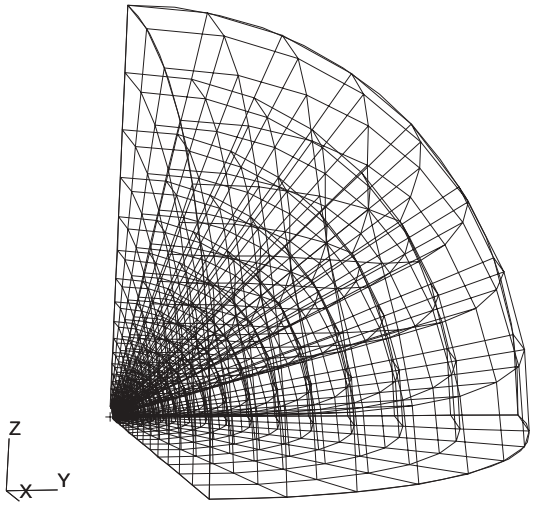

Figure 7b : FEM Model (NASTRAN) with 1159 Nodes for Boussinesq Problem

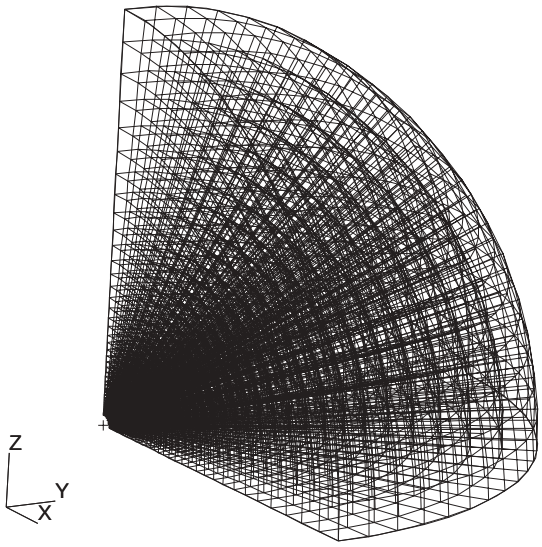

Figure 7d : FEM Model (NASTRAN) with 11112 Nodes for Boussinesq Problem

7.2 Eshelby's Inclusion Problem

The analytical solution for an elliptical inclusion, with eigenstrain in an infinite elastic medium was calculated by Eshelby in 1957. Remarkably, it turned out that the strain and stress fields inside the ellipsoid are uniform, and strain inside of the inclusion was related with the eigenstrain by Esheby's tensor. For simplicity, a spherical inclusion instead of an elliptical inclusion is simulated in this paper. The special treatment on the materials' interface, outlined in section 6.2 is applied to the problem of spherical inclusion in an infinite medium (Figure 10).

A uniform dilational eigenstrain is introduced into the

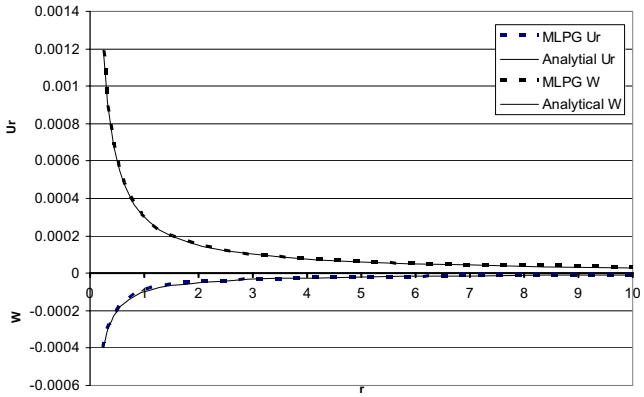

Figure 8a : Radial Displacement u_r and Vertical w Displacement at z = 0 for 3939 Node Model

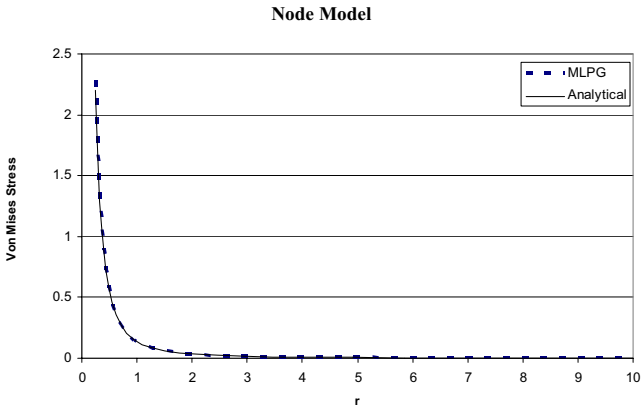

Figure 8b : Von Mises Stress at z = 0 for 3939 Node Model

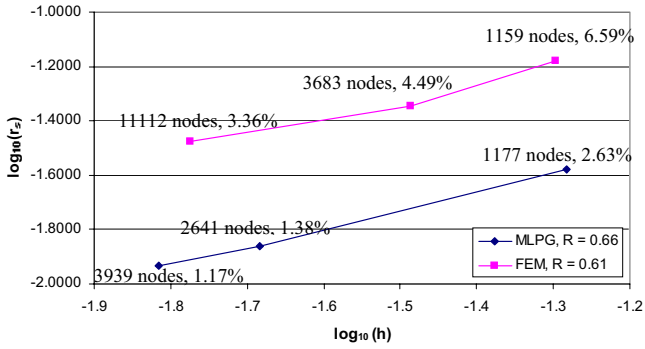

Figure 9a : Von Mises Stress Relative Error and Convergence Rate

spherical inclusion.

$$\varepsilon^*_{ij} = \varepsilon^{\alpha}\delta_{ij} \tag{42}$$

where ε^{α} is the magnitude of dilational strain. According to the analytical solution, the theoretical strain is given

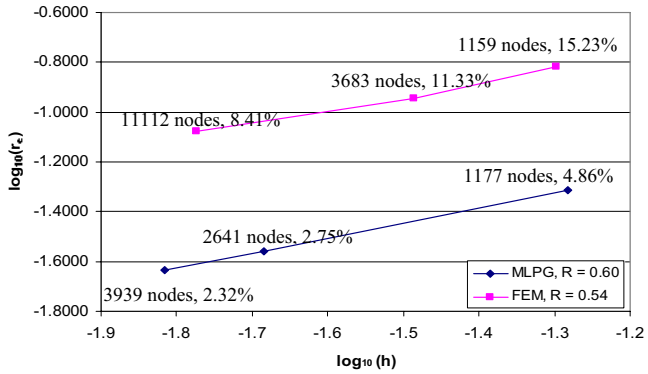

Figure 9b : Strain Energy Relative Error and Convergence Rate

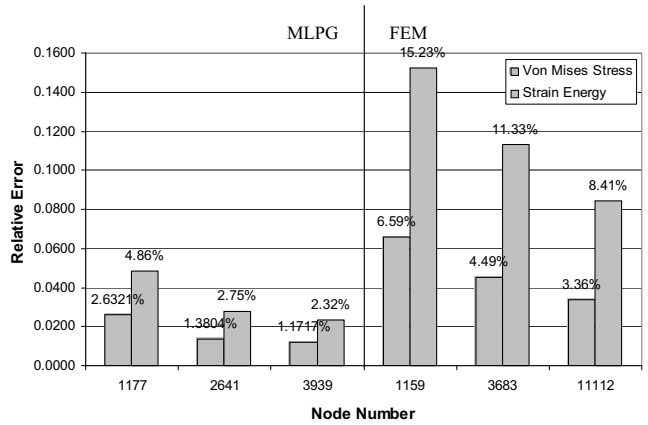

Figure 9c : Von Mises and Strain Energy Relative Error vs. Node Number

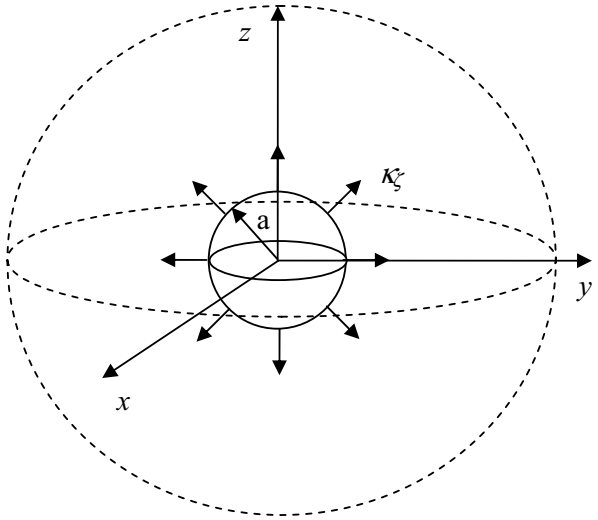

Figure 10 : Eshelby's Inclusion Problem

by [Mura (1982)]

$$\varepsilon_r = \varepsilon_t = \frac{1+\nu}{3(1-\nu)}\varepsilon^{\alpha} \qquad \text{Inside of the inclusion} \tag{43}$$

$$\begin{cases} \varepsilon_r = -\frac{2}{3}\frac{1+\nu}{(1-\nu)}\frac{a^3}{r^3}\varepsilon^{\alpha} \\ \varepsilon_t = \frac{1}{3}\frac{1+\nu}{(1-\nu)}\frac{a^3}{r^3}\varepsilon^{\alpha} \end{cases} \qquad \text{Outside of the inclusion} \tag{44}$$

where ε_r is the strain in the radial direction, ε_t is the strain in the tangential direction, ν is the Poisson's ratio, a is the radius of the spherical inclusion, and r is the distance to the center of the spherical inclusion. The analytical displacement is given by

$$\begin{cases} u_r = \frac{r(1+\nu)}{3(1-\nu)}\varepsilon^{\alpha} \\ u_t = 0 \end{cases} \qquad \text{Inside of the Inclusion} \tag{45}$$

$$\begin{cases} u_r = -\frac{2(1+\nu)}{3(1-\nu)}\frac{a^3}{r^3}\varepsilon^{\alpha} \\ u_t = 0 \end{cases} \qquad \text{Outside of the Inclusion} \tag{46}$$

It can be seen from the theoretical solution that while the displacement is continuous on the material interface, the radial strain shows an abrupt change at the inclusion boundary. In the current paper, the material properties used for numerical study are E = 100, ν = 0.3 for both the inclusion and the outside medium. The dilatational strain ε_{α} is set to be 0.01 inside the inclusion.

The infinite medium is represented by a sphere with a radius of 10, while the inclusion is represented with a small internal sphere with a radius of 2. Like the Boussinesq problem, only one-eighth of the sphere is used to represent the inclusion, as well as infinite medium (Figure 11). Symmetric boundary conditions are applied on the surface of one-eighth sphere, too. On the material interface of inclusion and infinite medium, two sets of nodes with different properties are placed on the same location in order to simulate the abrupt change in the strain field.

Three MLPG models using 1169, 2016 and 3892 nodes are used in the simulation. The 1169 node model has 127 node inside the inclusion and 1042 nodes outside the inclusion (Figure 12.a). The 2016 node model has 242 nodes inside the inclusion and 1774 nodes outside the inclusion. The 3892 node model has 746 nodes inside the inclusion and 3146 nodes outside the inclusion. For comparison purpose, three finite element models with 1591 nodes, 2789 nodes and 4401 nodes are also developed. A picture of the 4401 nodes model is shown in figure 12.b. Ten-node tetrahedral elements are used in the FEM analysis.

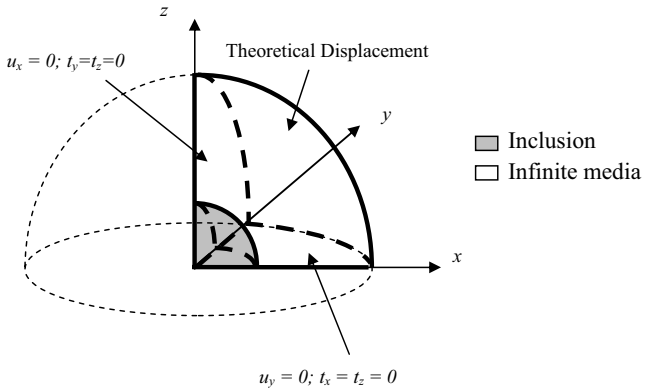

Figure 11 : Simulation Model for Eshelby's Inclusion Problem

The radial displacement, radial strain and hoop strain calculated from the 3892 node model with the MLPG method, and their comparison with analytical solutions, are shown in figure 13.a, 13.b and 13.c, respectively. It can be seen that with the presently proposed treatment of the material interface, the MLPG method is capable of simulating the abrupt change in the strain field with very high accuracy.

A convergence study is carried out for both the MLPG method and the FEM. The displacement relative error, and strain energy relative error, are plotted in figure 14.a and 14.b, respectively. The displacement relative errors of the MLPG method range from 0.30% to 3.39%. The strain energy relative errors of the MLPG method range from 0.64% to 4.72%. The convergence rate for the displacement relative error is 3.03. The convergence rate for the strain energy relative error is 2.51. The FEM results, on the other hand, give the similar accuracy in both the displacement and strain energy with the MLPG method. Furthermore, a better convergence rate is also observed when using the MLPG method. Therefore, we can summarize here that in spite of its highly continuous nature, the MLPG method can still achieve an accuracy that is

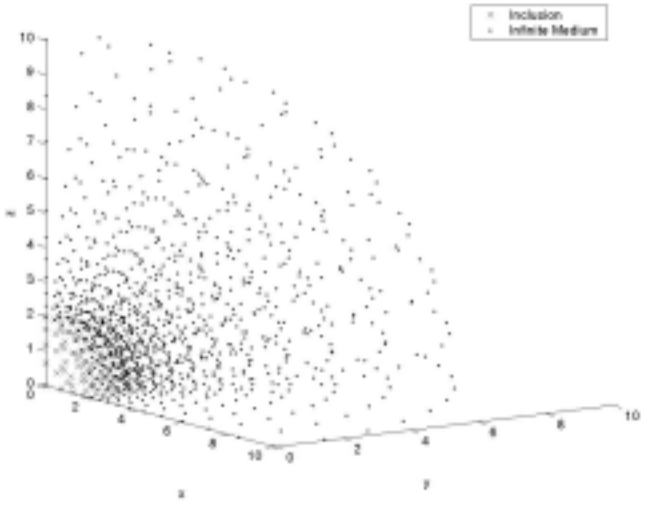

Figure 12a : Nodal Arrangement for Eshelby's Inclusion Problem (1169 nodes)

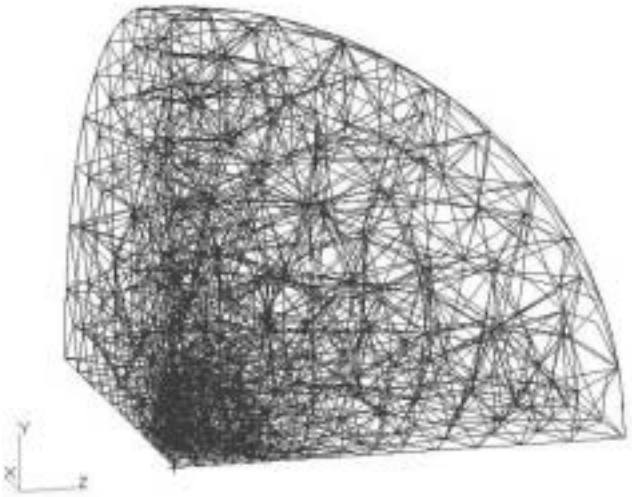

Figure 12b : FEM Model for Eshelby's Inclusion Problem (4401 nodes)

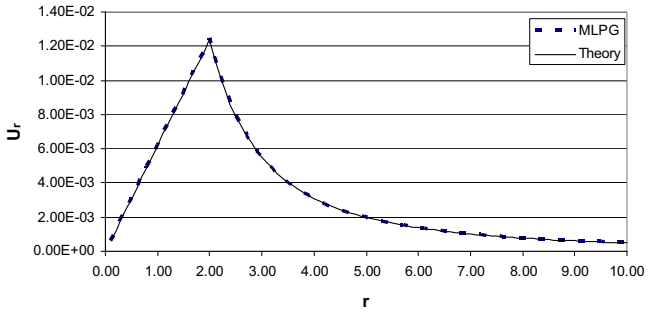

Figure 13a : Radial Displacement for the Inclusion Problem

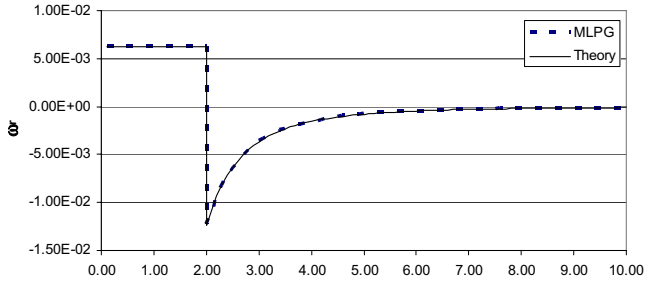

Figure 13b : Radial Strain for the Inclusion Problem

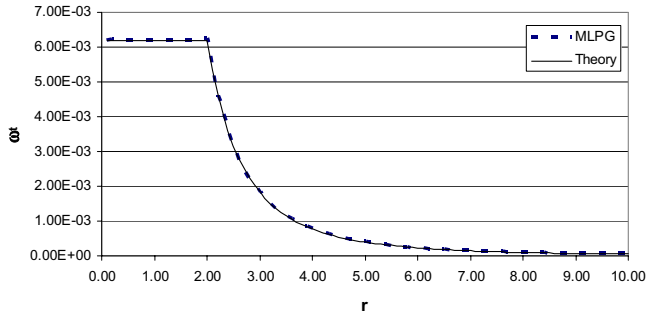

Figure 13c : Hoop Strain for the Inclusion Problem

comparable to the FEM method with the special treatment proposed in this paper.

8 Conclusion

An MLPG formulation of the three-dimensional elastostatic problem is presented in this paper. The current method is a truly meshless method, wherein no elements or background cells are involved, in either the interpolation or the integration. By properly choosing the test functions and trial functions, tedious geometric calculations are eliminated. The requirement for domain integration is minimized and even eliminated if no body forces are present. Hence, the calculation is accelerated and numerical requirement is significantly reduced. Furthermore, by choosing the Dirac's delta function as the test function on the material interfaces, the simulation of material discontinuities, which is a difficult task for other so-called meshless methods, is solved without any tedious numerical manipulation.

Unlike the other meshless methods, the current MLPG formulation has a straightforward physical interpretation as a simple enforcement of the overall momentum balance laws over each sub-domain Ω_s^I. This interpretation clearly paves the road for future development of nonlin-

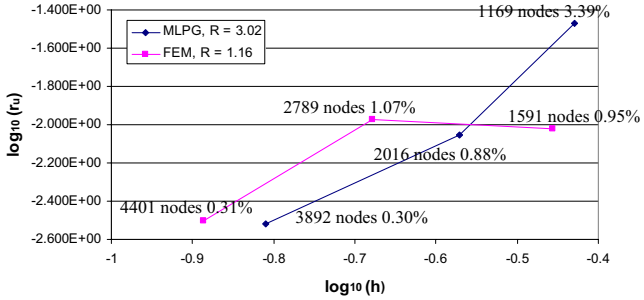

Figure 14a : Displacement Relative Error and Convergence Rate

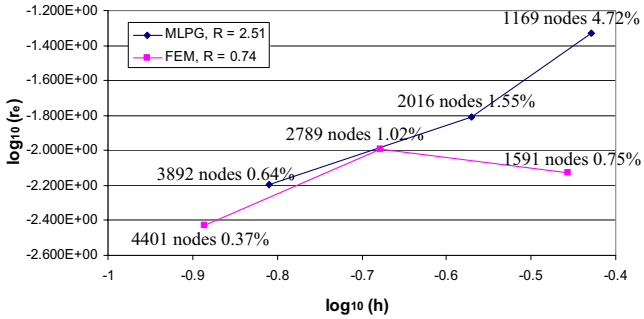

Figure 14b : Energy Relative Error and Convergence Rate

ear solid mechanics in solving large displacement gradients, large rotations, large strains and material inelastic behavior including plasticity, viscoplasticity, and creep.

The above methodology is applied to the Boussinesq problem, which is known to be a strongly singular problem. Compared with the finite element method, the current method achieves significantly higher accuracy with only one-third as many number of nodes, as compared to FEM. In order to demonstrate the performance of current method under a discontinuous strain field, Eshelby's inclusion problem is also analyzed. The current method shows excellent agreement with the analytical solution. A good convergence rate is observed, too.

The current MLPG method is proved to be a powerful tool for three-dimension elasto-static analysis. By using the simplifications and improvements introduced in this paper, the three dimensional MLPG method is capable of large scale calculation on models with complicated geometric configurations. Therefore, it is a very promising method that can possibly replace the finite element method in the near future.

Acknowledgement: This work was supported by the U. S. Army Research Office, and the U. S. Army Research Laboratory, under a cooperative research agreement with the University of California at Irvine. The Cognizant Program Official at the U. S. Army Research Labs is Dr. R. Namburu.

References

Atluri, S. N.; Zhu, T. (1998): A new meshless local Petrov-Galerkin (MLPG) approach in computational mechanics. *Comput. Mech.*, 22: 117-127

Atluri, S. N.; Kim, H. G.; Cho, J. Y. (1999): A critical assessment of the truly meshless local Petrov-Galerkin (MLPG) and Local Boundary Integral Equation (LBIE) methods. *Comput. Mech.*, 24: 348-372

Atluri, S. N.; Zhu, T. (2000): The meshless local Petrov-Galerkin (MLPG) approach for solving problems in elasto-statics. *Comput. Mech.*, 25: 169-179

Atluri, S. N.; Shen, S. P. (2002): The mesh local Petrov-Galerkin (MLPG) method: a simple & less-costly alternative to the finite element and boundary element methods. *CMES: Computer Modeling in Engineering & Sciences*, 3: 11-51

Atluri, S. N.; Shen, S. P. (2002): *The meshless local Petrov-Galerkin (MLPG) method.* Tech. Science Press.

Babuska, I.; Melenk, J. M. (1997): The partition of unity method. *Int. J. Num. Meth. Engrg.*, 40: 537-556

Barry, W.; Saigal, S. (1999): A three-dimensional element-free Galerkin elastic and elastoplastic formulation. *Int. J. Num. Meth. Engrg*, 46: 671-693

Batra, R. C.; Ching, H. K. (2002): Analysis of elastodynamic deformation near a crack/notch tip by the meshless local Petrov-Galerkin (MLPG) Method. *CMES: Computer Modeling in Engineering & Sciences*, 3(6): 717-730

Belytschko, T.; Lu, Y. Y.; Gu, L. (1994): Element free Galerkin methods. *Int. J. Num. Meth. Engrg.*, 37: 229-256

Breikopf, P.; Rassineux, A.; Touzot, G.; Villon, P. (2000): Explicit form and efficient computation of MLS shape functions and their derivatives. *Int. J. Num. Meth. Engrg.*, 48: 451-466

Ching, H. K.; Batra, R. C. (2001): Determination of crack tip fields in linear elastostatics by the meshless local Petrov-Galerkin (MLPG) method. *CMES: Computer*

Modeling in Engineering & Sciences, 2(2): 273-290

Cordes, L. W.; Moran, B. (1996): Treatment of material discontinuity in the element-free Galerkin method. *Comput. Meth. Appl. Mech. Engrg.*, 139: 75-89

Duarte, C.; Oden, J. T. (1996): HP-cloud – a meshless method to solve boundary value problems. *Comput. Meth. Appl. Mech. Engrg.*, 139: 237-262

Gu, Y. T.; Liu, G. R. (2001): A Meshless Local Petrov-Galerkin (MLPG) formulation for static and free vibration analysis of thin plate. *CMES: Computer Modeling in Engineering & Sciences*, 2(4): 463-476

Jin, X.; Li, G.; Aluru, N. R. (2001): On the equivalence between least-square and kernal approximations in meshless methods. *CMES: Computer Modeling in Engineering & Sciences*, 2(4): 447-462

Kim, H. G.; Atluri, S. N. (2000): Arbitrary placement of secondary nodes, and error control, in the meshless local Petrov-Galerkin (MLPG) method. *CMES: Computer Modeling in Engineering & Sciences*, 1(3): 11-32

Krongauz, Y.; Belytschko, T. (1998): EFG approximation with discontinuous derivatives. *Int. J. Numer. Meth. Engrg.*, 41: 1215-1233

Lin, H.; Atluri, S. N. (2000): Meshless local Petrov-Galerkin (MLPG) method for convection-diffusion problems. *CMES: Computer Modeling in Engineering & Sciences*, 1(2): 45-60

Lin, H.; Atluri, S. N. (2001): The meshless local Petrov-Galerkin (MLPG) method for solving incompressible Navier-Stokes equations. *CMES: Computer Modeling in Engineering & Sciences*, 2(2): 117-142

Liu, W. K.; Chen, Y.; Uras, R. A.; Chang, C. T. (1996): Generalized multiple scale reproducing kernel particle methods. *Comput. Meth. Appl. Mech. Engrg.*, 139: 91-157

Long, S.; Atluri, S. N. (2002): A meshless local Petrov-Galerkin (MLPG) method for solving the bending problem of a thin plane. *CMES: Computer Modeling in Engineering & Sciences*, 3(1): 53-64

Mukherjee, Y. X.; Mukherjee, S. (1997): On the boundary conditions in the element-free Galerkin method. *Comput. Mech.*, 19: 264-270

Mura, T. (1982): *Micromechanics of defects in solids.* Martinus Nijhoff Publishers, pp.75

Nayroles, B.; Touzot, G.; Villon, P. (1992): Generalizing the finite element method: diffuse approximation and diffuse elements. *Comput. Mech.*, 10: 307-318

Qian, L. F.; Batra, R. C.; Chen, L. M. (2003): Elastostatic deformations of a thick plate by using a higher-order shear and normal deformable plate theory and two Meshless Local Petrov-Galerkin (MLPG) methods. *CMES: Computer Modeling in Engineering & Sciences*, 4(1): 161-176

Raju, I. S.; Phillips, D. R. (2003): Further developments in the MLPG method for beam problems. *CMES: Computer Modeling in Engineering & Sciences*, 4(1): 141-160

Sladek, J.; Sladek, V.; Atluri, S. N. (2001): A pure contour formulation for the meshless local boundary integral equation method in thermoelasticity. *CMES: Computer Modeling in Engineering & Sciences*, 2(4): 423-434

Tang, Z.; Shen, S.; Atluri, S. N. (2003): Analysis of materials with strain-gradient effects: A meshless local Petrov-Galerkin (MLPG) approach, with nodal displacements only. *CMES: Computer Modeling in Engineering & Sciences*, 4(1): 177-196

Timoshenko; Goodier (1951): *Theory of elasticity.* McGraw-Hill Book Company, pp.362

Zhu, T.; Atluri, S. N. (1998): A modified collocation method and a penalty formulation for enforcing the essential boundary conditions in the element free Galerkin method. *Comput. Mech.*, 21: 211-222